Quaternary Science Reviews 256 (2021) 106841

Contents lists available at ScienceDirect

Quaternary Science Reviews

journal homepage: www.elsevier.com/locate/quascirev

Beryllium isotopes in sediments from Lake Maruwan Oike and Lake Skallen, East Antarctica, reveal substantial glacial discharge during the late Holocene

Adam D. Sproson [a, b, *], Yoshinori Takano [b], Yosuke Miyairi [a], Takahiro Aze [a], Hiroyuki Matsuzaki [c], Naohiko Ohkouchi [b], Yusuke Yokoyama [a, b, d, e]

[a] Atmosphere and Ocean Research Institute (AORI), The University of Tokyo, Japan
[b] Biogeochemistry Research Center (BGC), Japan Agency for Marine-Earth Science and Technology (JAMSTEC), Yokosuka, Japan
[c] Micro Analysis Laboratory, Tandem Accelerator (MALT), The University of Tokyo, Japan
[d] Department of Earth and Planetary Science, Graduate School of Science, The University of Tokyo, Japan
[e] Graduate Programme on Environmental Science, University of Tokyo, Komaba, Meguro, Tokyo, Japan

ARTICLE INFO

Article history:
Received 22 January 2021
Accepted 4 February 2021
Available online 23 February 2021

Handling Editor: C. O'Cofaigh

Keywords:
Beryllium
Glacial discharge
Subglacial weathering
Lützow-Holm bay
East Antarctic Ice Sheet
Holocene

ABSTRACT

Constraining East Antarctic Ice Sheet (EAIS) evolution during the Holocene is important for exploring the forcing mechanisms behind ice sheet retreat and to constrain numerical ice sheet models that aid predictions of future sea-level rise. Beryllium (Be) isotope analysis of bedrock and marine sediments have offered unparalleled insight into Antarctic ice sheet history since the Pliocene, but much of EAIS remains poorly studied. Here, we report the reactive (authigenic) ^{10}Be abundance, ^{9}Be abundance and ^{10}Be/^{9}Be ratios of Antarctic lake sediments, for the first time, from Lake Maruwan Oike and Lake Skallen along Soya Coast of Lützow-Holm Bay, East Antarctica. Beryllium isotope records reveal melting of local glaciers associated with higher subglacial erosion between ~4.1 and ~3.6 ka BP. Comparison to marine records from the Antarctic continental shelf suggests this was part of a circum-Antarctic phenomena that led to widespread glacial discharge from other sectors of the East and West Antarctic Ice Sheet. We suggest the incursion of relatively warm Circumpolar Deep Water (CDW) into Lützow-Holm Bay during the Late Holocene led to frontal and basal melting of ice sheets along the Soya Coast, supporting the notion of Antarctic ice sheet instabilities as a contributor to global sea-level rise since the Mid Holocene.

1. Introduction

The EAIS is the largest continental ice sheet on Earth, with a volume equivalent to ~53 m in mean sea-level spanning a vast continental area from ~45°W to ~168°E (Fig. 1A) (Fretwell et al., 2013; Lythe and Vaughan, 2001). The EAIS responds to feedbacks associated with changing ice elevation, planetary albedo and atmospheric circulation (DeConto and Pollard, 2016; Pollard and DeConto, 2009) and can strongly influence global sea-level, oceanic temperature and circulation (Flower and Kennett, 1994). Although the EAIS is considered to be relatively stable when compared to the West Antarctic and Greenland Ice Sheets, its retreat history since the Last Glacial Maximum (LGM) suggests deglacial pulses from the Lambert/Amery glacial system, ~18 kyr ago, and in Mac. Robertson Land, ~14 kyr ago, followed by more widespread recession between ~12 kyr and 6 kyr ago (Mackintosh et al., 2014). However, the evolution of the EAIS during the Mid (8.2 ka BP to 4.2 ka BP) and Late (4.2 ka BP to present) Holocene, and its potential contribution to global sea level is not well constrained (Gehrels, 2010). Diatom oxygen isotope records ($\delta^{18}O_{diatom}$) suggest an increase in glacial discharge from Prydz Bay and Adélie Land since ~4.5 ka BP (Crespin et al., 2014; Crosta et al., 2018), but vast areas of East Antarctica remain poorly studied. Further contributions are required to determine the evolution of the EAIS during the Holocene and the mechanism by which it changed, such as atmospheric-driven melting, ocean-driven melting, ice sheet instabilities and/or ice shelf instabilities, if we are to better constrain the numerical modelling of its response to present-day and future climatic change (Bentley et al., 2014; DeConto and Pollard, 2016;

* Corresponding author. Atmosphere and Ocean Research Institute (AORI), The University of Tokyo, Japan.
E-mail addresses: adamsproson@gmail.com, sproson@aori.u-tokyo.ac.jp, sproson@aori.u-tokyo.ac (A.D. Sproson).

https://doi.org/10.1016/j.quascirev.2021.106841
0277-3791/

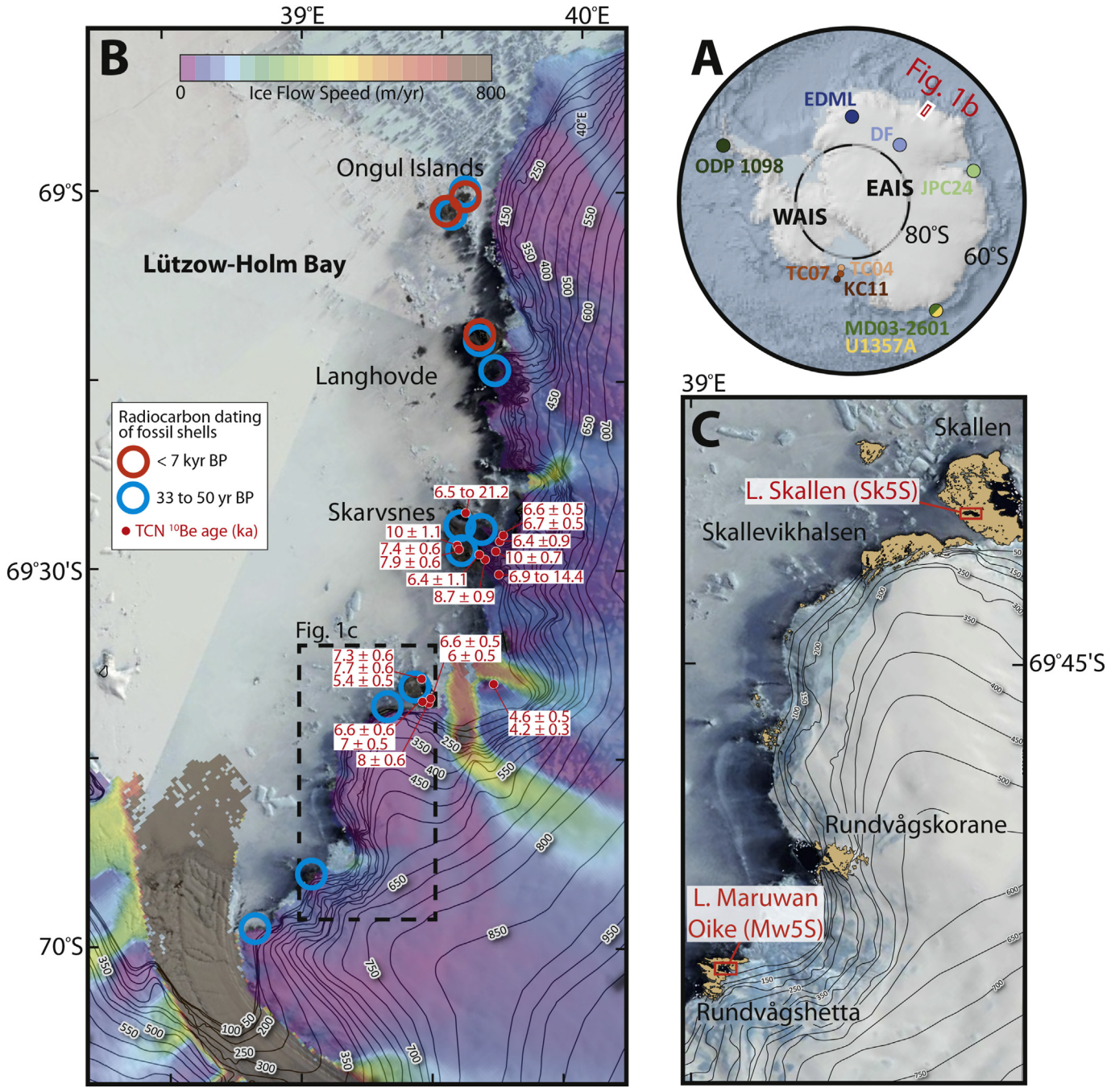

Fig. 1. (**A**) Map of Antarctica displaying the location of EDML (EPICA Dronning Maud Land) and DF (Dome Fuji) ice core drilling sites (Masson-Delmotte et al., 2011) and JPC24 (Prydz Bay), MDO3-2601 (Adélie Land), U1357A (Adélie Land), TC04 to KC11 (Ross Sea) and ODP 1098 (west Antarctic Peninsula) marine sediment cores (Behrens et al., 2019; Crespin et al., 2014; Crosta et al., 2018; Pike et al., 2013; Yokoyama et al., 2016) relative to Lützow-Holm Bay, Dronning Maud Land (red square). (**B**) Ice velocity (Mouginot et al., 2012; Rignot et al., 2011), satellite imagery (Bindschadler et al., 2008), radiocarbon dates and total cosmogenic nuclide (TCN) dates (Kawamata et al., 2020; Mackintosh et al., 2014; Yamane et al., 2011) for Lützow-Holm Bay. (**C**) Location of Lake Maruwan Oike and Lake Skallen (red squares) along the Soya Coast. Maps were made using Quantarctica from the Norwegian Polar Institute (Matsuoka et al., 2018). (For interpretation of the references to colour in this figure legend, the reader is referred to the Web version of this article.)

Mackintosh et al., 2014).

The cosmogenic isotope ^{10}Be is produced by the interaction of cosmic rays with oxygen and silicon in silicate minerals at the Earth's surface ("*in situ*" production), or oxygen and nitrogen in the atmosphere ("meteoric" production), which subsequently deposits to the Earth's surface via precipitation or dust (Lal, 1991; Willenbring and von Blanckenburg, 2010). In-situ ^{10}Be is produced in glacial erratics and bedrock after the retreat of overlying ice, allowing calculated exposure ages to determine past ice sheet elevations and the timing of deglaciations (e.g., Johnson et al., 2014; Jones et al., 2017; Kawamata et al., 2020; Lilly et al., 2010; Mackintosh et al., 2014; Nishiizumi et al., 1991; Small et al., 2019; Spector et al., 2017; Yamane et al., 2015; Yamane et al., 2011). Meteoric ^{10}Be is deposited to marine sediments directly from the atmosphere after ice shelf retreat, which has been utilised to constrain the timing of the Ross Ice Shelf collapse (Scherer et al., 1998; Sjunneskog et al., 2007; Yokoyama et al., 2016), or from Antarctic meltwater during warming events, revealing periods of

high meltwater discharge from the Wilkes subglacial basin (Behrens et al., 2019; Valletta et al., 2018). Together these applications of the Be isotope system have provided unparalleled insight into Antarctic ice sheet history since the Pliocene.

When meteoric ^{10}Be is normalised to the stable isotope ^{9}Be, released from silicate minerals during weathering, the resulting ^{10}Be/^{9}Be ratios of the reactive (authigenic) phase of fluvial and marine sediments reflects the ratio of freshwater inputs to silicate weathering flux, and has been used to quantify runoff, erosion rates and denudation on both a regional and global scale (Rahaman et al., 2017; von Blanckenburg and Bouchez, 2014; Von Blanckenburg et al., 2015; von Blanckenburg et al., 2012; Wittmann et al., 2012). When applied to lacustrine sediments, from Laguna Potrok Aike (Argentina) and Lake Hovsgol (Mongolia), the authigenic ^{10}Be/^{9}Be record has been used to reconstruct local hydrological conditions and climate induced variations in runoff and sediment input since the LGM (Choi et al., 2014; Kim et al., 2012). Despite this potential, Antarctic authigenic ^{10}Be/^{9}Be records remain sparse, having only been applied to marine sediments from the Ross Sea (Sjunneskog et al., 2007), offshore Wilkes Land (Valletta et al., 2018) and Prydz Bay (White et al., 2019), and have yet to be measured in Antarctic lake sediments.

We report ^{10}Be abundance, ^{9}Be abundance and ^{10}Be/^{9}Be ratios for the reactive phase of sediments from Lake Maruwan Oike (sample code: Mw5S) and Lake Skallen (sample code: Sk5S) positioned along the Soya Coast of Lützow-Holm Bay (Fig. 1), East Antarctica, to test the applicability of Be isotopes as a proxy for meltwater discharge and subglacial weathering since the Mid Holocene. Beryllium isotope records are combined with major element abundances from the literature and a new age-depth model to explore the sources and timing of Be input to the Soya Coast. Finally, the ^{10}Be/^{9}Be ratios from Lake Maruwan Oike and Lake Skallen are compared to Mid-to-Late-Holocene paleoclimatic records from the Southern Hemisphere to explore potential environmental implications.

2. Regional setting

Lützow-Holm Bay (Fig. 1B) is a discharge point for one of East Antarctica's major drainage basins (Anderson et al., 2002; Rignot et al., 2013) which includes the Shirase Glacier and a number of smaller glaciers (Miura et al., 1998; Verleyen et al., 2017). Several islands and ice-free peninsulas are situated within the bay, composed primarily of granites, metabasites, and gneisses with beds of marble and quartzite (Tatsumi and Kizaki, 1969). Carbon-14 ages of fossil shells in raised beaches can be divided into either pre-LGM (33–40 ka BP) or Holocene (<7 ka BP) ages (Mackintosh et al., 2014; Miura et al., 1998; Takada et al., 2003) and suggest the EAIS retreated to the Ongul Islands and northern Langhovde by 30–46 ka BP with subsequent post-LGM retreat to Skallen and Skarvsnes during the Holocene (Fig. 1B). These interpretations are supported by ^{26}Al and ^{10}Be exposure ages of glacial erratics (Kawamata et al., 2020; Yamane et al., 2011) which suggest the Skallen and Skarvsnes peninsula became ice-free between 10 and 5 ka BP (Fig. 1B).

Sawagaki and Hirakawa (1997) have described the evidence of past sub-glacial meltwater flow channels and erosional bedforms at Rundvågshetta and Skallen. After the ice-retreat events of the Holocene, a number of freshwater and saline lakes became situated on ice-free peninsulas along the Soya Coast (Imura et al., 2003; Kudoh and Tanabe, 2014). Lake Maruwan Oike (hereafter L. Maruwan Oike) is situated on Rundvågshetta (Fig. 1C), a rock headland at the southwest margin of the Rundvåg Glacier (Takano et al., 2015). Lake Skallen (hereafter L. Skallen) is 1180 m long and situated in central Skallen (Fig. 1C), a 14.1 km^2 ice-fee coastal area of rocky hills close to the Skallen Glacier (Takano et al., 2012). Both lakes are marine relict lakes fed by meltwater from a relatively large catchment of snow and ice located on the coastal side of their respective peninsulas (Kudoh and Tanabe, 2014). Lakes Maruwan Oike and Skallen are separated from the open ocean by sills (outflow points) with respective heights of 8 m (Institute, 1984) and 9.64 ± 0.02 m above mean sea level (AMSL), having been isolated by glacio-isostatic uplift at 3471 ± 90 cal yr BP and 2940 ± 100 cal yr BP, respectively (Takano et al., 2012, 2015). Prior to isolation, sediments from L. Maruwan Oike and L. Skallen record marine conditions extending back to 6010 ± 140 cal yr BP and 5295 ± 133 cal yr BP, respectively (Takano et al., 2012, 2015). Both lakes have a reported ice-thickness of <2 m.

3. Material and methods

3.1. Core sampling and description

Sediments were collected using push-type corers (diameter, < 8 cm) during the 47th Japanese Antarctic Research Expedition (JARE47; from December 2005 to January 2006 for the field survey). The corer equipped with a core-catcher is believed to have penetrated to the bedrock of L. Skallen and 156 and 360 cm of core were recovered from lakes Maruwan Oike and Skallen, respectively. The cores were cut into 3–10 cm intervals and stored at 0 to 4 °C for geochemical analysis (Shiraishi, 2007; Takano et al., 2010) and −20 °C for microbiological analysis (Watanabe et al., 2013). Both cores generally consist of a laminated microbial mat with silt and clay layers interspersed with thicker layers of aluminium-rich mud or fine sand (see Fig. 2; Takano et al., 2015; Takano et al., 2012). We selected samples every 4 to 20 and 10 to 40 cm, equating to an average of a sample every 300 and 370 cal yr BP, in lakes Maruwan Oike and Skallen, respectively (Table 1).

3.2. Beryllium isotope analysis

The technique for separation of reactive Be from sediments is based on Bourles et al. (1989). In brief, ~0.1 g of dried and crushed sediment was leached using 2 ml of 0.04 M hydroxylamine hydrochloride (NH_2OH–HCl) in 25% acetic acid for 7 h at 80 °C. The resulting leachate was dissolved in 14 N HNO_3 + 12 N $HClO_4$ (4 ml: 2 ml), evaporated to dryness, and then dried to ~1 ml using 14 N HNO_3 + 9 N HCl (4 ml: 2 ml). The resulting solution was diluted to 20 ml using deionized (Milli-Q™) water, of which a 2 ml aliquot was sampled for the measurement of reactive ^{9}Be abundance. The remaining solution was spiked with 1 ml of a 0.097 mg/ml ^{9}Be carrier in order to accurately determine ^{10}Be sample concentrations from the measured ^{10}Be/^{9}Be ratios. Beryllium was purified using two solvent extractions of acetylacetone in the precedence of EDTA (Bourles et al., 1989) followed by the precipitation of $Be(OH)_2$ with NH_4 (Kohl and Nishiizumi, 1992). The resulting hydroxide was dried in a quartz vial and converted to BeO using a microwave ceramic crucible for 5 min (Yokoyama et al., 2019c). The BeO powder was mixed with niobium (Nb) and inserted into a copper cathode ready for the measurement of reactive ^{10}Be abundance (Yokoyama et al., 2019c).

The reactive ^{10}Be abundances were measured by a National Electrostatic Corporation (NEC) accelerator mass spectrometer (AMS), of 5 MV terminal voltage, at the University of Tokyo (UTokyo), Micro Analysis Laboratory, Tandem accelerator (MALT) (Matsuzaki et al., 2007). Absolute values were obtained using the KNB5-1 standard (^{10}Be/^{9}Be = 2.997 × 10^{-11}; Nishiizumi et al., 2007) with a typical beam current of 2–5 μA (^{9}Be^{16}O^{-}; Yokoyama et al., 2019c). The natural authigenic ^{9}Be abundances were measured using a Thermo® ELEMENT XR high resolution inductively coupled plasma mass spectrometer (HR-ICP-MS) at the Atmosphere and

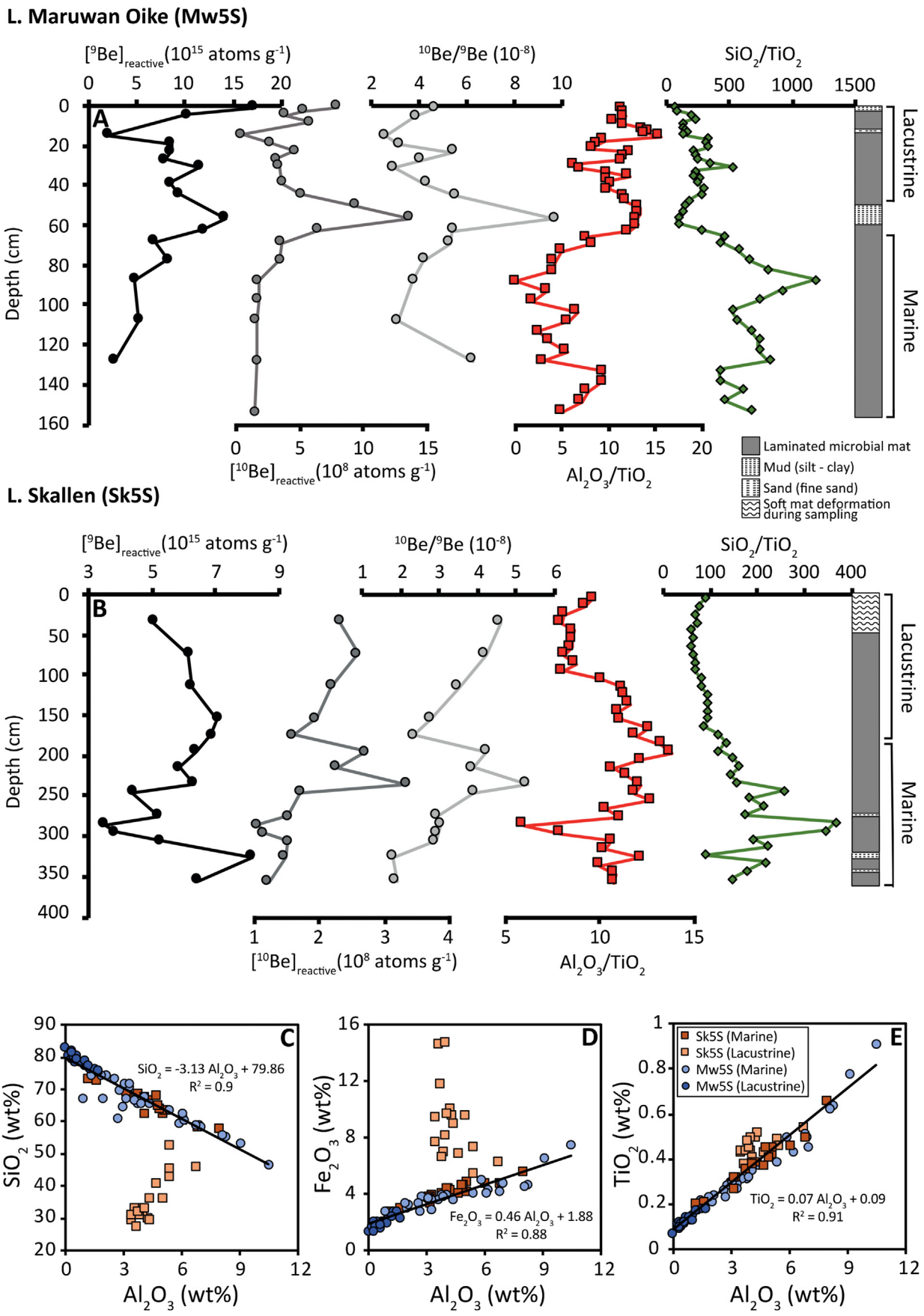

Fig. 2. The reactive ^{9}Be abundance, ^{10}Be abundance and $^{10}Be/^{9}Be$ ratios (this study) alongside lithological descriptions, Al_2O_3/TiO_2 ratios and SiO_2/TiO_2 ratios (Takano et al., 2012, 2015) for Lake Maruwan Oike (**A**) and Lake Skallen (**B**). Diagram of Al_2O_3 vs. SiO_2 (**C**), Al_2O_3 vs. Fe_2O_3 (**D**) and Al_2O_3 vs. TiO_2 (**E**) for Lake Maruwan Oike (Takano et al., 2015) and Lake Skallen (Takano et al., 2012).

Ocean Research Institute (AORI), UTokyo, after spiking with 5 μl of indium (1 μg/g) solution to correct for matrix effects (Knudsen et al., 2008; Sproson et al., 2021). The calculated authigenic ^{9}Be, ^{10}Be and $^{10}Be/^{9}Be$ ratios (Table 1) for L. Maruwan Oike and L. Skallen are presented in Fig. 2 along with bulk major element profiles (SiO_2, Al_2O_3, Fe_2O_3 and TiO_2) previously determined using X-ray fluorescence by Takano et al. (2015) and Takano et al. (2012), respectively.

3.3. Age-depth model

Four samples from L. Skallen, at a mid-depth of 215, 255, 295 and 335 cm, were chemically prepared for radiocarbon (^{14}C) measurement of organic carbon following procedures presented previously (Yokoyama et al., 2007). The ratio between $^{14}C/^{12}C$ was quantified using Accelerator Mass Spectrometry (AMS) at the University of Tokyo (Yokoyama et al., 2019b) and final radiocarbon ages are presented in Table 1. New radiocarbon ages were compiled with ages previously obtained from L. Maruwan Oike (Takano et al., 2015) and L. Skallen (Takano et al., 2012) sediments. Previously, radiocarbon ages were converted to calendar ages using the calibration program Calib Rev (Stuiver et al., 1998) and the Marine09 and IntCal09 calibration curves (e.g., Hughen et al., 2004; Reimer et al., 2009). However, classic approaches to age-depth modelling assume no uncertainty for the depth value of dated intervals. As an accurate age model is vital for determining the timing of Be isotope variations new calendar ages (Table 1) and a new age-depth model (Fig. 3) was calculated using the modelling routine, *Undatable*, which used the Bayesian ^{14}C calibration software, *MatCal*, to take into account depth uncertainties of 10 cm (Table 1) and analytical uncertainty associated with ^{14}C measurement (Lougheed and Obrochta, 2019). Calendar ages were recalibrated using the SHCal13 and Marine13 international calibration datasets (Hogg et al., 2013; Reimer et al., 2013) for the terrestrial and marine section of each lake, respectively (Verleyen et al., 2017). A respective marine reservoir effect (ΔR) of 1300 yr and 1100 yr for marine stage sequences of lakes Maruwan Oike and Skallen was used, based on ^{14}C dating of core-top samples and the flesh and shells of living marine benthic organisms (Hayashi and Yoshida, 1994; Ingólfsson et al., 1998; Miura et al., 2002). *Undatable* was run for 10^6 iterations for both cores using a Gaussian SAR uncertainty factor of 0.1 and a bootstrapping percentage of 40%, due to the high number of age reversals found in L. Maruwan Oike (Fig. 3).

4. Results

4.1. Be isotope records for L. Maruwan Oike and L. Skallen

The $[^{9}Be]_{reactive}$ and $[^{10}Be]_{reactive}$ of sediments recorded here (Table 1) range from 2.02 to 17.18 $\times$ 10^{15} atoms/g (mean = 7.24 $\times$ 10^{15} atoms/g; σ = 3.25) and 0.52 to 13.64 $\times$ 10^{8} atoms/g (mean = 3.1 $\times$ 10^{8} atoms/g; σ = 2.54). The $[^{9}Be]_{reactive}$ values generally fall below Antarctic estimates from offshore Wilkes Land of 16.9–27.2 $\times$ 10^{15} atoms/g (Valletta et al., 2018) but compare well to values of 8–42.8 $\times$ 10^{15} atoms/g in Prydz Bay (White et al., 2019) and 5.9–32.7 $\times$ 10^{15} atoms/g in other bodies of water draining glacial systems such as Baffin Bay, offshore Greenland (Simon et al., 2016). The $[^{10}Be]_{reactive}$ values compare well to other Antarctic regions such as offshore Wilkes Land and Prydz Bay at respective values of 1.3–12.7 and 0.15–11.1 $\times$ 10^{8} atoms/g but far lower than values recorded in paleolake sediments from the Antarctic Dry Valleys of 0.03–150 $\times$ 10^{5} atoms/g (Valletta et al., 2015). We compile new Be isotope records with previously recorded major element profiles (Takano et al., 2012, 2015) to identify key trends and elucidate the major controls on Be isotope variation.

Since the formation of L. Maruwan Oike and L. Skallen around 5400 years ago (Fig. 3), deposition of silt and clay layers with greenish-greyish organic-rich laminations have recorded subglacial weathering processes and local meltwater inputs from nearby glaciers (Takano et al., 2012, 2015). The Al_2O_3/TiO_2 ratios in L. Maruwan Oike (Fig. 2A) and L. Skallen (Fig. 2B) indicate higher weathering rates and detrital inputs under brackish to lacustrine conditions (<62.5 cm) and marine to lacustrine conditions (115–355 cm), respectively. However, Al_2O_3/TiO_2 ratios also show a negative correlation to SiO_2/TiO_2 ratios (green diamonds in Fig. 2), an indicator of marine productivity, in L. Maruwan Oike (Fig. 2A) and the marine section of L. Skallen (Fig. 2B) suggesting Al_2O_3/TiO_2 ratios may be controlled by the relative mixing of a freshwater, subglacial, endmember (High Al_2O_3 and TiO_2) and a marine endmember (Low Al_2O_3 and TiO_2) (Fig. 2E). The mixture of these two endmembers in L. Maruwan Oike and the marine section of L. Skallen is illustrated by the relationship of SiO_2 vs. Al_2O_3 (Fig. 2C) which is defined by high biogenic silica and diatom abundance relative to low terrestrial Al inputs under marine conditions (Takano et al., 2012, 2015). The reduction in SiO_2 to ~30 wt% in the lacustrine section of L. Skallen is caused by low productivity under anoxic conditions. This mixing trend is also reflected in SiO_2/TiO_2 ratios (green diamonds in Fig. 2), a relative indicator of the biogenic component of lake sediments, which record seawater incursions at 87.5 and 127.5 cm in L. Maruwan Oike and at 285 cm in L. Skallen, with generally higher ratios under marine conditions (Fig. 2A and B).

Reactive ^{9}Be (black circles in Fig. 2) is positively correlated to Al_2O_3/TiO_2 and Al_2O_3/Fe_2O_3 ratios in L. Maruwan Oike above 23 cm ($[^{9}Be]_{reactive}$ = 0.53 Al_2O_3/TiO_2 + 3.9, R^2 = 0.51; $[^{9}Be]_{reactive}$ = 4.77 Al_2O_3/Fe_2O_3 + 4.98, R^2 = 0.57) and L. Skallen ($[^{9}Be]_{reactive}$ = 0.39 Al_2O_3/TiO_2 + 1.73, R^2 = 0.43; $[^{9}Be]_{reactive}$ = 2.16 Al_2O_3/Fe_2O_3 + 3.92, R^2 = 0.32) suggesting $[^{9}Be]_{reactive}$ in sediments is largely controlled by the relative amount of Be released during weathering, as previously shown (Simon et al., 2016; von Blanckenburg and Bouchez, 2014; von Blanckenburg et al., 2012; Wittmann et al., 2012). In L. Maruwan Oike, $[^{9}Be]_{reactive}$ gradually increases from 4.81 $\times$ 10^{15} atoms/g at 87.5 cm to 14.13 $\times$ 10^{15} atoms/g at 56.5 cm along with an increase in Al_2O_3/TiO_2 and a decrease in SiO_2/TiO_2 indicating peak subglacial weathering and freshwater discharge during the brackish transition from marine to lacustrine conditions (Fig. 2A). In L. Skallen, $[^{9}Be]_{reactive}$ is generally high (5.86–8.15 $\times$ 10^{15} atoms/g) between 155 cm and 325 cm at times of high Al_2O_3/TiO_2 ratios, indicating more intense subglacial weathering during this time, but with a superimposed trough in $[^{9}Be]_{reactive}$ at ~285 cm caused by the incursion of seawater, as indicated by high SiO_2/TiO_2 ratios (Fig. 2B). The $[^{10}Be]_{reactive}$ values (dark grey circles in Fig. 2) are positively correlated with $[^{9}Be]_{reactive}$ (R^2 = 0.64), Al_2O_3 (R^2 = 0.4) and TiO_2 (R^2 = 0.43) in L. Maruwan Oike and $[^{9}Be]_{reactive}$ (R^2 = 0.3 when excluding samples at 235 and 325 cm) in L. Skallen suggesting a similar terrestrial source.

4.2. Age-depth model

According to the new age-depth model for cores from lakes Maruwan Oike and Skallen, respective sedimentation began at $4,945^{+231}_{-167}$ and $5,412^{+133}_{-109}$ cal yr BP (Fig. 3), similar to previous estimates of 4807 to 5204 and 5293–5559 cal yr BP (Takano et al., 2012, 2015) and consistent with other lakes along the Soya Coast

Table 1
Depth, ^{14}C age, calendar age and beryllium isotope measurements for Lake Maruwan Oike and Lake Skallen.

Depth (cm)	Mid-depth (cm)	^{14}C age (yr BP)[a]	2σ	Calendar age (cal yr BP)[b]	$[^{10}Be]_{reactive}$ (10^8 atoms g^{-1})	2σ	$[^{9}Be]_{reactive}$ (10^{15} atoms g^{-1})	2σ	$^{10}Be/^{9}Be$ (10^{-8})	2σ
Lake Maruwan Oike (MW5s)										
0–2	1	–	–	80^{+391}_{-354}	7.98	0.59	17.18	0.10	4.64	0.37
2–4	3	–	–	497^{+1040}_{-309}	5.27	0.55	–	–	–	–
4–6	5	–	–	879^{+1379}_{-493}	3.92	0.39	10.24	0.06	3.83	0.40
6–8	9	–	–	1612^{+1296}_{-877}	5.83	0.32	–	–	–	–
14–16	15	–	–	2285^{+843}_{-705}	0.52	0.20	2.02	0.01	2.57	1.01
18–20	19	–	–	2749^{+467}_{-348}	2.71	0.37	8.63	0.15	3.15	0.48
22–24	23	–	–	3084^{+217}_{-438}	4.65	0.24	8.61	0.13	5.39	0.36
26–28	27	–	–	3270^{+127}_{-520}	3.17	0.36	7.93	0.28	4.00	0.60
30–32	31	–	–	3325^{+181}_{-482}	3.37	0.24	11.43	0.13	2.95	0.24
38–40	39	–	–	3378^{+250}_{-335}	3.65	0.37	8.51	0.13	4.29	0.50
43–46	44.5	–	–	3419^{+276}_{-185}	5.11	0.61	9.28	0.08	5.51	0.70
49–52	50.5	–	–	3502^{+263}_{-128}	9.39	0.25	–	–	–	–
55–58	56.5	–	–	3609^{+214}_{-174}	13.64	0.82	14.13	0.01	9.65	0.59
61–64	62.5	–	–	3703^{+180}_{-221}	6.43	0.44	11.87	0.09	5.42	0.41
67–70	68.5	–	–	3801^{+159}_{-280}	3.60	0.43	6.86	0.02	5.25	0.64
75–80	77.5	–	–	3899^{+177}_{-323}	3.48	0.39	8.28	0.01	4.20	0.47
85–90	87.5	–	–	3953^{+333}_{-313}	1.81	0.08	4.81	0.03	3.77	0.20
95–100	97.5	–	–	4004^{+449}_{-286}	1.79	0.36	–	–	–	–
105–110	107.5	–	–	4058^{+507}_{-240}	1.63	0.31	5.22	0.06	3.11	0.63
125–130	127.5	–	–	4163^{+618}_{-182}	1.70	0.34	2.74	0.00	6.23	1.25
150–156	153	–	–	4945^{+231}_{-167}	1.57	0.42	–	–	–	–
Lake Skallen (Sk5S)										
30–40	35	–	–	471^{+115}_{-119}	2.32	0.39	5.06	0.04	4.59	0.80
70–80	75	–	–	1154^{+323}_{-237}	2.59	0.58	6.16	0.07	4.21	0.99
110–120	115	–	–	1841^{+418}_{-462}	2.19	0.37	6.26	0.03	3.51	0.61
150–160	155	–	–	2544^{+242}_{-510}	1.95	0.29	7.06	0.07	2.77	0.43
170–180	175	–	–	2758^{+361}_{-272}	1.61	0.51	6.87	0.05	2.35	0.77
190–200	195	–	–	3063^{+378}_{-198}	2.72	0.43	6.40	0.11	4.24	0.75
210–220	215	4665	60	3443^{+311}_{-324}	2.28	0.25	5.86	0.05	3.88	0.45
230–240	235	–	–	3768^{+259}_{-407}	3.34	0.21	6.32	0.02	5.29	0.34
240–250	245	–	–	3954^{+213}_{-461}	1.73	0.47	4.40	0.03	3.92	1.10
250–260	255	5240	70	4131^{+188}_{-492}	–	–	–	–	–	–
270–280	275	–	–	4305^{+250}_{-368}	1.53	0.37	5.21	0.04	2.93	0.74
280–290	285	–	–	4376^{+314}_{-280}	1.07	0.36	3.52	0.03	3.05	1.06
290–300	295	5405	50	4466^{+343}_{-212}	1.14	0.24	3.83	0.03	2.98	0.66
300–310	305	–	–	4595^{+328}_{-186}	1.53	0.20	5.24	0.03	2.93	0.40
320–330	325	–	–	4845^{+290}_{-172}	1.48	0.36	8.15	0.07	1.81	0.46
330–340	335	5820	50	4975^{+253}_{-156}	–	–	–	–	–	–
350–360	355	–	–	5309^{+142}_{-123}	1.23	0.29	6.46	0.06	1.90	0.46

[a] Measured in this study.
[b] Calculated using ^{14}C ages from this study and Takano et al. (2012; 2015) using *undateable*

(Rudd, 2019; Rudd et al., 2016; Verleyen et al., 2017) and surface exposure ages (Fig. 1B) which estimate the Skarvsnes and Skallen peninsula were deglaciated by ~5 ka BP (Kawamata et al., 2020; Yamane et al., 2011). Diatom assemblages, biogenic opal-A and molecular analysis reveal a transition from marine to lacustrine settings in L. Maruwan Oike, between 50 and 65 cm, and L. Skallen, at 185 cm (Takano et al., 2012, 2015). Using our new age-depth model, this corresponds to an age of $3,493^{+267}_{-125}$ to $3,744^{+168}_{-245}$ cal yr BP and $2,872^{+402}_{-172}$ cal yr BP for L. Maruwan Oike and L. Skallen, respectively (Fig. 3). This is similar to previous respective estimates for lakes Maruwan Oike and Skallen of 3382 to 3560 and 2800 to 3063 cal yr BP (Takano et al., 2012, 2015).

5. Discussion

5.1. $[^{9}Be]_{reactive}$ records terrestrial inputs and subglacial weathering processes

The stable isotope ^{9}Be is concentrated in silicate minerals and released during weathering (von Blanckenburg and Bouchez, 2014; Wittmann et al., 2012), displaying a similar relationship in lakes to other weathering products such as Al, Fe and Ti (Choi et al., 2014). The $[^{9}Be]_{reactive}$ records (black circles in Fig. 2) from lakes Maruwan Oike and Skallen display a similar trend to Al_2O_3/TiO_2 (red squares in Fig. 2) and are positively correlated to Al_2O_3/TiO_2 and Al_2O_3/Fe_2O_3 suggesting ^{9}Be is terrestrially sourced from local freshwater

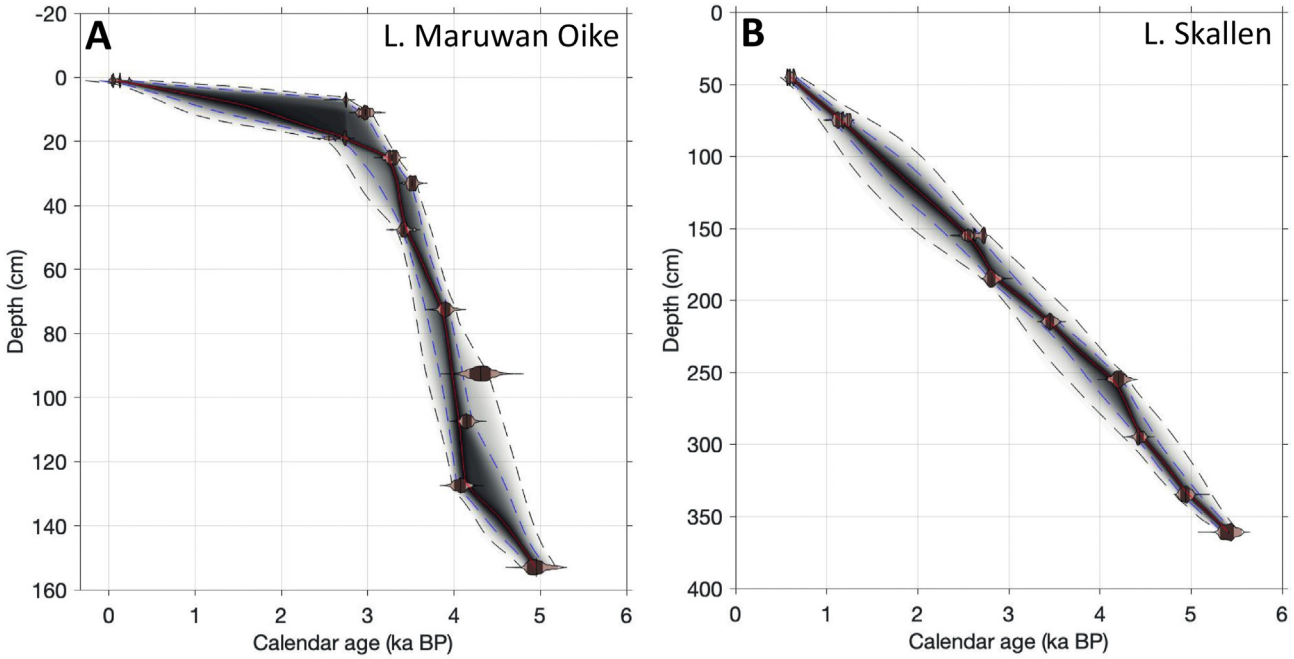

Fig. 3. *Undatable* age-depth model for Lake Maruwan Oike (**A**) and Lake Skallen (**B**) based on ^{14}C dates from this study (Table 1), Takano et al. (2015) and Takano et al. (2012). The red line, blue broken line and black broken line represents the median, 1σ confidence and 2σ confidence intervals, respectively. (For interpretation of the references to colour in this figure legend, the reader is referred to the Web version of this article.)

inputs (see section 4.1).

Titanium, Al and Fe are considered to be relatively immobile during weathering processes and the relative abundances of these elements in sediments have been used to indicate changes in weathering provenance and depositional history (Young and Nesbitt, 1998). The relationship of Fe_2O_3 vs. Al_2O_3 (Fig. 2D) and TiO_2 vs. Al_2O_3 (Fig. 2E) for L. Maruwan Oike and the marine section of L. Skallen display a weathering profile ($Fe_2O_3 = 0.46\ Al_2O_3 + 1.88$, $R^2 = 0.88$; $TiO_2 = 0.07\ Al_2O_3 + 0.09$, $R^2 = 0.91$) indicative of moderately weathered and sorted material sourced from the same catchment area draining an identical underlying bedrock (Brown, 2002; Young and Nesbitt, 1998). The lacustrine section of L. Skallen displays an elevated abundance of Fe_2O_3 relative to Al_2O_3, which may suggest a switch to more anoxic conditions (light brown squares in Fig. 2D). Widespread anoxia in the cyanobacteria-rich saline L. Skallen is supported by higher MnO, MnO/Fe_2O_3, total carbon, total nitrogen and total sulphur under lacustrine conditions, high levels of which are not recorded in the *Chaetoceros*-based diatom-rich freshwater of L. Maruwan Oike (Melles et al., 2012; Minyuk et al., 2014; Sapota et al., 2006; Takano et al., 2012, 2015).

Despite anoxic conditions, the TiO_2 vs. Al_2O_3 relationship remains relatively constant, although slightly enriched in TiO_2 likely due to delivery of more fine-grained material under lacustrine conditions in L. Skallen (Minyuk et al., 2014; Whitlock et al., 2008), suggesting a consistent weathering provenance throughout the deglacial history of both lakes (Fig. 2E). The Al_2O_3/TiO_2 ratios of both L. Maruwan Oike and L. Skallen (red squares in Fig. 2) will therefore reflect the relative levels of subglacial weathering intensity, with preferential removal of Al from bedrock under higher physical and chemical weathering rates, and detrital input (Young and Nesbitt, 1998). This implies ^9Be inputs to both lakes are sourced from an identical catchment area throughout their history related to the subglacial weathering of the nearby Rundvåg and Skallen glaciers, displaying elevated weathering rates and detrital inputs from 1 to 5 cm and 19–77.5 cm in L. Maruwan Oike and 115–235 cm and 325–355 cm in L. Skallen (Fig. 2).

5.2. The $[^{10}Be]_{reactive}$ of lake sediments reflects local meltwater inputs

The cosmogenic nuclide ^{10}Be is produced in the upper atmosphere and deposited to the ocean where it mixes with fluvial ^{10}Be leading to a ^{10}Be abundance of 170–2000 atoms/g with an average abundance of 770 ± 80 atoms/g in South Atlantic surface waters (Brown et al., 1992; Frank et al., 2009; Ku et al., 1990; Kusakabe et al., 1987; Measures et al., 1996). Incursions of seawater, as evidenced by high SiO_2/TiO_2 ratios, in L. maruwan Oike and L. Skallen under marine conditions would therefore introduce marine ^{10}Be to underlying sediments. However, the $[^{10}Be]_{reactive}$ records of both lakes are not correlated with SiO_2/TiO_2 ratios, instead displaying some of their lowest ^{10}Be abundances during periods of highest SiO_2/TiO_2 values (Fig. 2A and B). As direct atmospheric fallout of ^{10}Be to L. Maruwan Oike and L. Skallen is negligible (see section 4.4 for more details), another source is needed to drive $[^{10}Be]_{reactive}$ to higher values. The $[^{10}Be]_{reactive}$ values are positively correlated with $[^9Be]_{reactive}$ ($R^2 = 0.64$), Al_2O_3 ($R^2 = 0.4$) and TiO_2 ($R^2 = 0.43$) in L. Maruwan Oike and $[^9Be]_{reactive}$ ($R^2 = 0.3$ when excluding samples at 235 and 325 cm) in L. Skallen, whilst being negatively correlated to the relative amounts of biogenic opal-A (Takano et al., 2012, 2015), suggesting $[^{10}Be]_{reactive}$ is largely controlled by subglacial, freshwater, inputs.

The ^{10}Be abundance of Antarctic ice sheets ranges from 5 to 8×10^4 atoms/g (Baroni et al., 2011; Raisbeck et al., 2007; Raisbeck and Yiou, 1985), several orders of magnitude higher than seawater, and largely controls the ^{10}Be abundance of Antarctic marine sediments through meltwater discharge (Behrens et al., 2019; Valletta et al., 2018). The $[^{10}Be]_{reactive}$ of sediments from L. Maruwan Oike and L. Skallen are therefore most likely controlled by the relative amounts of meltwater input from the nearby Rundvåg Glacier and

Skallen Glacier, respectively (Fig. 1C). Both L. Maruwan Oike and L. Skallen display a single peak in $[^{10}Be]_{reactive}$ at respective depths of 56.5 cm and 195–235 cm, suggesting enhanced meltwater discharge at this time (Fig. 2A and B). This is generally associated with higher terrestrial input of ^{9}Be, Al_2O_3, Fe_2O_3 and TiO_2 associated with enhanced subglacial weathering along the Soya Coast.

5.3. High $^{10}Be/^{9}Be$ ratios reveal local meltwater discharge between 4.1 and 3.6 ka BP

The ratio of the meteoric cosmogenic nuclide ^{10}Be to the stable isotope ^{9}Be in the ocean, recorded in the reactive phase of marine sediments, has been proposed as a flux proxy of terrigenous input, whereby shifts in fluvial discharge, and therefore weathering flux, will result in shifts of $^{10}Be/^{9}Be$ ratios (von Blanckenburg and Bouchez, 2014; Von Blanckenburg et al., 2015). The ^{10}Be and ^{9}Be abundances recorded here are largely controlled by the respective freshwater discharge and subglacial weathering of nearby glaciers, suggesting the $^{10}Be/^{9}Be$ ratio of the reactive phase of Antarctic lake sediments may also be used as a flux proxy of terrigenous input in a similar manner to marine sediments and temperate lakes (Choi et al., 2014; Kim et al., 2012; Simon et al., 2016; Valletta et al., 2018). When compiled onto the new age depth models presented here (Fig. 3), both L. Maruwan Oike (black circles in Fig. 4A) and L. Skallen (grey squares in Fig. 4A) display a similar variation in $^{10}Be/^{9}Be$ ratios through the Mid to Late Holocene. The $^{10}Be/^{9}Be$ ratios of Lake Skallen increase from 1.8 to 2.9 between 4.8 and 4.6 ka BP, remaining constant for ~300 years, before increasing again from 2.9 to 5.3 between 4.3 and 3.8 ka BP simultaneously with an increase from 3.1 to 9.7 in L. Maruwan Oike between 4.1 and 3.6 ka BP (Fig. 4A). Both lakes undergo a rapid decline in $^{10}Be/^{9}Be$ ratios to pre-excursion values by ~2.8 ka BP before gradually increasing towards present day values (Fig. 4A).

Previous Be analysis of marine cores from the Atlantic and Pacific have shown the relationship between relative $[^{10}Be]_{reactive}$ and $[^{9}Be]_{reactive}$ concentrations are largely controlled by extraction efficiency, scavenging efficiency or dilution, with changes in the gradient of this relationship above or below one indicating superimposed variability in $[^{9}Be]$ or $[^{10}Be]$, respectively (Von Blanckenburg et al., 2015). The relationship of relative $[^{10}Be]_{reactive}$ vs. relative $[^{9}Be]_{reactive}$ for L. Maruwan Oike (black circles in Fig. 4B) and L. Skallen (grey squares in Fig. 4B) are largely defined by slopes equal to one. This suggests the $^{10}Be/^{9}Be$ ratios of L. Maruwan Oike and L. Skallen are generally controlled by extraction efficiency, scavenging efficiency or dilution, with no dominant control from ^{10}Be or ^{9}Be variability. Despite these general trends, both lakes deviate towards a $[^{10}Be]_{reactive}$ vs. $[^{9}Be]_{reactive}$ relationship similar to marine sediments from offshore Wilkes Land (open diamonds in Fig. 4B) defined by a slope less than one (dashed line in Fig. 4B), corresponding to peak $^{10}Be/^{9}Be$ ratios in L. Maruwan Oike, at 3609^{+214}_{-176} cal yr BP, and L. Skallen, at $3,768^{+259}_{-407}$ cal yr BP (Fig. 4A) indicative of an excess influx of ^{10}Be to both lakes. At offshore Wilkes Land this relationship is interpreted to reflect the retreat of the glacial margin during Pliocene warming events introducing additional ^{10}Be through meltwater discharge (Valletta et al., 2018). It is therefore proposed that the rapid rise in $^{10}Be/^{9}Be$ ratios between 4.1 ka BP and 3.6 ka BP recorded here (Fig. 4A) is likely due to a release in meltwater during the retreat of the Rundvåg and Skallen glaciers.

5.4. Estimating denudation rates and meltwater flux from Be isotopes

Previous work by von Blanckenburg et al. (2012) and von Blanckenburg and Bouchez (2014) created a conceptual scaffold for the $^{10}Be/^{9}Be$ system at the Earth Surface and in the oceans. Concerning a river and at steady-state, if there is sufficient contact time between river particulates and river water as expected in subglacial systems of the Shirase and Soya Drainage Basins, the Be isotope ratio of the dissolved phase of river waters, $(^{10}Be/^{9}Be)_{diss}$, is equivalent to the isotope ratio of reactive phase of river waters, $(^{10}Be/^{9}Be)_{reac}$, defined by the following ratio (von Blanckenburg and Bouchez, 2014):

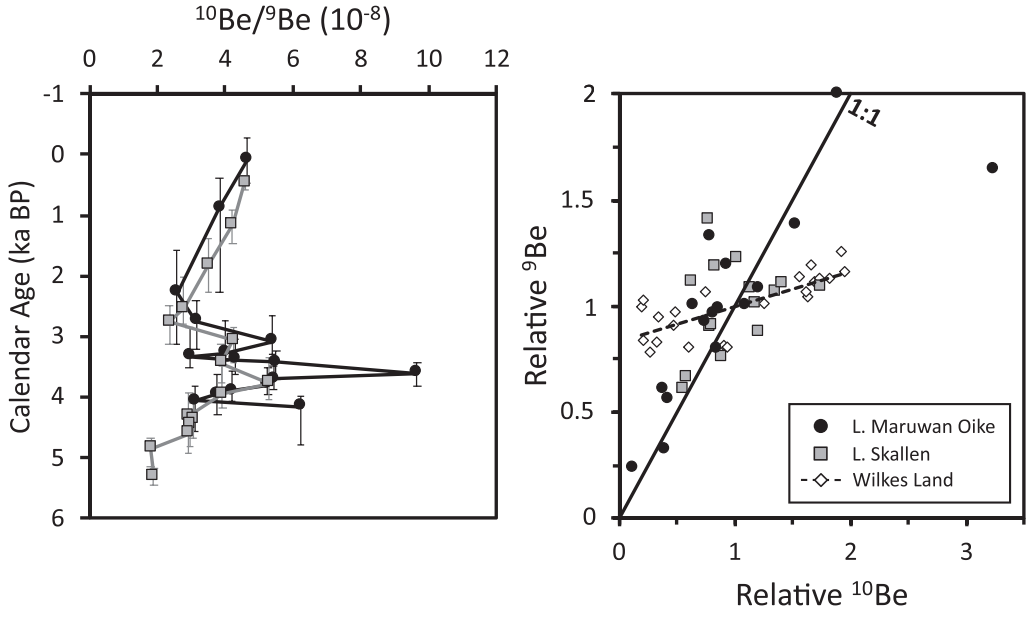

Fig. 4. The $^{10}Be/^{9}Be$ ratios (**A**) and relative ^{10}Be vs. relative ^{9}Be relationship (**B**) for Lake Maruwan Oike (black circles) and Lake Skallen (grey squares). Values from offshore Wilkes Land for Pliocene interglacials (Valletta et al., 2018) are displayed using open diamonds.

$$\left(\frac{^{10}Be}{^{9}Be}\right)_{reac} = \left(\frac{^{10}Be}{^{9}Be}\right)_{diss} = \frac{F_{riv}^{^{10}Be}}{D \cdot \left[^{9}Be\right]_{parent} \cdot \left(f_{reac}^{^{9}Be} + f_{diss}^{^{9}Be}\right)} \quad (1)$$

where $F_{riv}^{^{10}Be}$ describes the flux of meteoric ^{10}Be received by the river basin (in atoms/m^2/yr), D is the denudation rate (in kg/m^2/yr), $\left[^{9}Be\right]_{parent}$ is the ^{9}Be concentration of the river basins parent rock (in atoms/kg) and $f_{reac}^{^{9}Be} + f_{diss}^{^{9}Be}$ is the fraction of ^{9}Be released from the parent rock during weathering (von Blanckenburg and Bouchez, 2014; von Blanckenburg et al., 2012). Equation (1) is applicable for describing the Be isotope ratio of lakes with a surface area far lower than the area of the surrounding catchment area (von Blanckenburg and Bouchez, 2014) such as L. Maruwan Oike and L. Skallen which have a relatively small area (0.21–0.25 km^2) relative to the surrounding Soya Drainage Basin (10^5 km^2) (Kudoh and Tanabe, 2014; Nakamura et al., 2016).

Unlike precipitation dominated lakes described in equation (1), the Antarctic catchment area is dominated by meltwater flux from local glaciers and, following Behrens et al. (2019), $F_{riv}^{^{10}Be}$ therefore becomes $T_{melt} \cdot \rho_{ice} \cdot \left[^{10}Be\right]_{ice}$ giving the following equation defining the ^{10}Be/^{9}Be ratio of glacially terminating lakes:

$$\left(\frac{^{10}Be}{^{9}Be}\right)_{reac} = \left(\frac{^{10}Be}{^{9}Be}\right)_{diss} = \frac{T_{melt} \cdot \rho_{ice} \cdot \left[^{10}Be\right]_{ice}}{D \cdot \left[^{9}Be\right]_{parent} \cdot \left(f_{reac}^{^{9}Be} + f_{diss}^{^{9}Be}\right)} \quad (2)$$

where T_{melt} is the total amount of meltwater released from glaciers (in cm^3/yr), ρ_{ice} is the density of ice (0.9 g/cm^3) and $\left[^{10}Be\right]_{ice}$ is the meteoric ^{10}Be concentration of the ice sheet (in atoms/g) (Behrens et al., 2019). Given the area of the lake, A_{basin} (in cm^2), the sedimentation rate, R_{sed} (in cm/yr), and sediment density, ρ_{sed} (in g/cm^3), the ^{10}Be concentration of the reactive phase of lake sediments, $\left[^{10}Be\right]_{sed}$ (in atoms/g), at the time of deposition can be defined as follows (Behrens et al., 2019):

$$\left[^{10}Be\right]_{sed} = \frac{T_{melt} \cdot \rho_{ice} \cdot \left[^{10}Be\right]_{ice}}{A_{basin} \cdot R_{sed} \cdot \rho_{sed}} \quad (3)$$

and the ^{9}Be concentration of the reactive phase of lake sediments, $\left[^{9}Be\right]_{sed}$ (in atoms/g), at the time of deposition can be defined as:

$$\left[^{9}Be\right]_{sed} = \frac{D \cdot \left[^{9}Be\right]_{parent} \cdot \left(f_{reac}^{^{9}Be} + f_{diss}^{^{9}Be}\right)}{A_{basin} \cdot R_{sed} \cdot \rho_{sed}} \quad (4)$$

Using a ρ_{sed} of 2 g/cm^3 (Verleyen et al., 2017), $\left[^{9}Be\right]_{parent}$ of 4.2×10^{22} atoms/g for mafic rocks (von Blanckenburg et al., 2012), the underlying lithology of the Soya coast, a global $f_{reac}^{^{9}Be} + f_{diss}^{^{9}Be}$ of 0.2 (von Blanckenburg and Bouchez, 2014), a $\left[^{10}Be\right]_{ice}$ of 5×10^4 atoms/g (Raisbeck et al., 2007), a respective A_{basin} of 0.25 km^2 and 0.21 km^2 (Kudoh and Tanabe, 2014) and R_{sed} of 0.1 and 0.06 cm/yr, calculated from the new age-depth model, for L. Maruwan Oike and L. Skallen we can use equations (2)–(4) to determine the meltwater flux (T_{melt}) and denudation rate (D) needed to produce the ^{10}Be/^{9}Be ratio, ^{10}Be abundance and ^{9}Be abundance recorded in the reactive phase of L. Maruwan Oike and L. Skallen during the Holocene.

The most striking variation in the ^{10}Be/^{9}Be ratios of L. Maruwan Oike and L. Skallen occurs between ~4.1 and ~3.6 ka BP (Fig. 4A). A denudation rate of 0.32 and 0.15 kg/yr and a meltwater flux of 18.4×10^{11} and 8×10^{11} cm^3/yr gives a $\left[^{10}Be\right]_{sed}$, $\left[^{9}Be\right]_{sed}$ and ^{10}Be/^{9}Be$_{reac}$ comparable to measured values at $4,058^{+507}_{-240}$ and $4,305^{+250}_{-368}$ for L. Maruwan Oike and L. Skallen, respectively (Table 1). A denudation rate of 0.8 and 0.18 kg/yr and a meltwater flux of 15.2×10^{12} and 18.4×10^{11} cm^3/yr gives a $\left[^{10}Be\right]_{sed}$, $\left[^{9}Be\right]_{sed}$ and ^{10}Be/^{9}Be$_{reac}$ comparable to measured values at $3,609^{+214}_{-174}$ and $3,768^{+259}_{-407}$ for L. Maruwan Oike and L. Skallen, respectively (Table 1). This suggests a respective increase in the annual flux of meltwater of 730 and 130% and eroded material of 150 and 20% between ~4.1 and ~3.6 ka BP to L. Maruwan Oike and L. Skallen, respectively. Although the calculated meltwater flux is relatively small, if the nearby Shirase glacier, which has a contemporary basal melt rate of 5.7 Gt/yr (Rignot et al., 2013), experienced the same level of enhanced melting at 3.6 ka BP it would signify a significant contribution to glacial eustacy during the Late Holocene.

5.5. Atmospheric or oceanic forcing as a driver of Antarctic variability

Beryllium isotope data from L. Maruwan Oike and L. Skallen indicate increased glacial melting along the Soya Coast from 4.1 to 3.6 ka BP and from ~2.8 ka BP to the present (Fig. 5A). This compares well to $\delta^{18}O_{diatom}$ records (Fig. 5B) from Prydz Bay, Adélie Land, George V Land and the west Antarctic Peninsula (Fig. 1A) which decrease from ~5 ka BP to the present due to the input of δ^{18}O-depleted glacial meltwater (Crespin et al., 2014; Crosta et al., 2018; Pike et al., 2013). Centennial events of low $\delta^{18}O_{diatom}$ at ~4.2 ka BP, ~3.2 to 2.3 ka BP and 1.9 to 0.9 ka BP in Prydz Bay, ~4 ka BP, ~3 to 2.5 ka BP and ~1.8 ka BP in Adélie Land and George V Land, and ~4.3 ka BP and 2.5 ka BP to present on the west Antarctic Peninsula (Fig. 5B) compare well to periods of peak glacial meltwater release recorded here (Fig. 5A). This is further supported by a release of meltwater ^{10}Be from the Wilkes subglacial basin (Fig. 1A) between 4 and 2 ka BP and from ~1.5 ka BP (Fig. 5C) (Behrens et al., 2019). At the same time the Ross Ice Shelf began to retreat at ~5 ka BP, reaching its final configuration by ~1.5 ka BP (Fig. 5D) (Yokoyama et al., 2016). Taken together, these studies suggest circum-Antarctic glacial discharge since ~4.5 ka BP indicating a common driving mechanism for Antarctic climatic change during the Late Holocene.

Explanations for melting of marine terminating glaciers on the Antarctic Peninsula and Wilkes Land often invoke atmospheric warming from increased El Niño-Southern Oscillation (ENSO) variability and a greater occurrence of La Niña events relative to El Niño events since ~5 ka BP (Crespin et al., 2014; Pike et al., 2013). Lacustrine records from Ecuador (Moy et al., 2002) and the Galápagos (Conroy et al., 2008) indicate a stepwise rise in ENSO variability at ~4.2 ka BP and 2 ka BP (Fig. 5E) around the same time as higher ^{10}Be/^{9}Be ratios in L. Maruwan Oike and L. Skallen (Fig. 5A). However, despite the observed cyclicity in Antarctic ice core records indicating millennial scale warming events linked to internal oscillations within the climate system (Masson et al., 2000), δ^{18}O records from the EPICA Dronning Maud Land (Fig. 5F) and Dome Fuji (Fig. 5G) ice cores, closest to Lützow-Holm Bay (Fig. 1A), indicate a general cooling trend from ~4.5 ka BP (Crosta et al., 2018; Masson-Delmotte et al., 2011) with no evidence of warming at the time of high ^{10}Be/^{9}Be ratios (Fig. 5A). This suggests a rise in surface air temperature and moisture delivery over Antarctica linked to movements of the South Pacific Convergence Zone (Pike et al., 2013), teleconnected to ENSO circulation via the Amundsen Sea

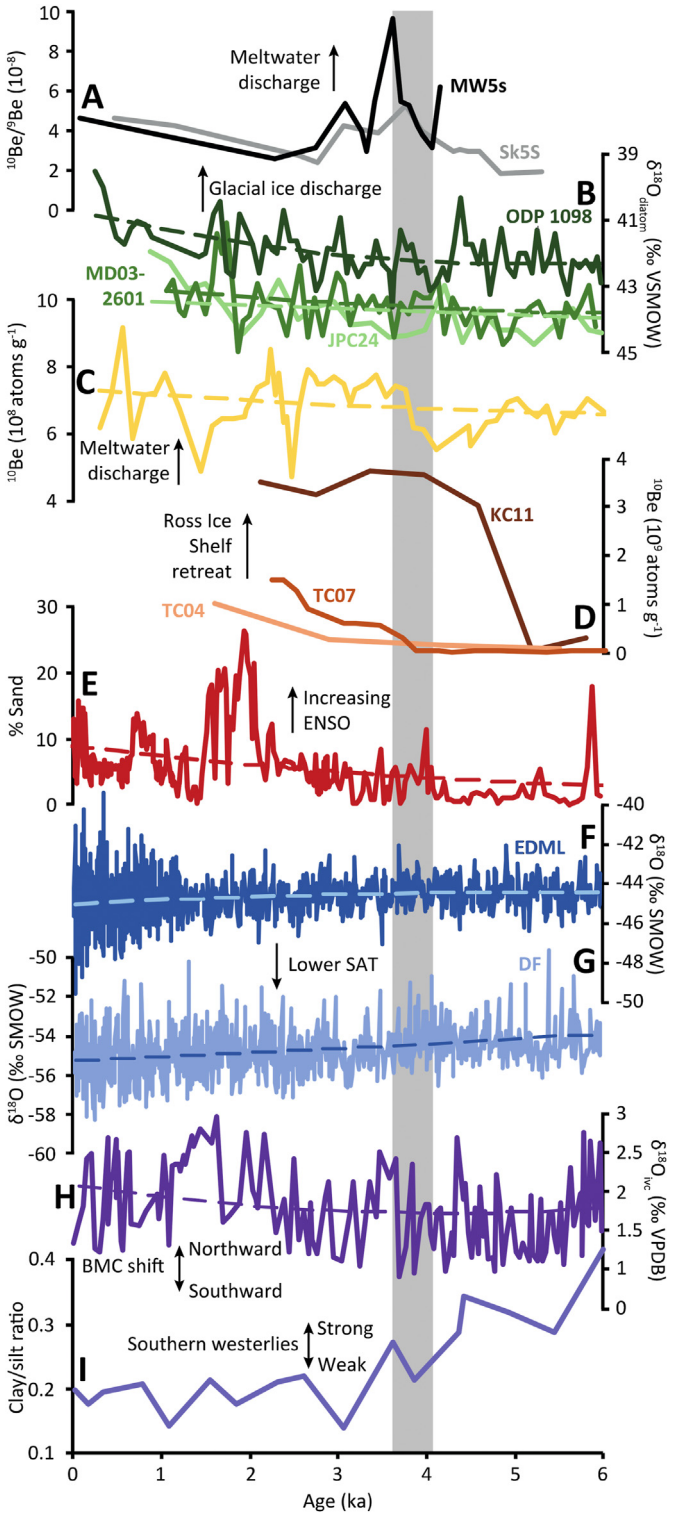

Fig. 5. Proxy records illustrating possible Antarctic forcing mechanisms for the Late Holocene. Meltwater and glacial ice discharge reconstruction from (**A**) $^{10}Be/^{9}Be$ ratios (this study), (**B**) $\delta^{18}O_{diatom}$ (Crespin et al., 2014; Crosta et al., 2018; Pike et al., 2013) and (**C**) ^{10}Be abundances (Behrens et al., 2019). (**D**) Ross Ice Shelf retreat history from ^{10}Be abundances (Yokoyama et al., 2016). (**E**) Percentage of Sand in the El Junco Crater Lake, Galápogos (Conroy et al., 2008). Oxygen isotope records for EPICA Dronning Maud Land (**F**) and Dome Fuji (**G**) ice cores reflecting changes in surface air temperature (SAT) over the EAIS (Masson-Delmotte et al., 2011). (**H**) Position of the Brazil-Malvinas Confluence (BMC), a highly sensitive feature of the SWW, reconstructed from an ice volume corrected *Globorotalia inflata* $\delta^{18}O$ ($\delta^{18}O_{ivc}$) record of the South Atlantic (Voigt et al., 2015). (**I**) Clay/silt ratios from Skyring 1 Southern Chile (Lamy et al., 2010). Antarctic records correspond to filled circles in Fig. 1A. The grey box highlights 4.1 ka BP to 3.6 ka BP corresponding to the most dramatic rise in $^{10}Be/^{9}Be$ ratios recorded in this study. Dashed lines represent a 2nd order polynomial best fit to the data.

low-pressure region, is unlikely to be the main cause of meltwater discharge to the Soya Coast.

Alternatively, a recent modelling study suggested an increase in Southern Ocean subsurface water temperature from ~6 ka BP, due to higher summer insolation at high latitudes and enhanced upwelling of CDW onto the Antarctic continental shelf, caused ice front and basal melting leading to the observed variation in $\delta^{18}O_{diatom}$ records from Prydz Bay, Adélie Land, George V Land and the west Antarctic Peninsula (Fig. 5B) since ~5 ka BP (Crosta et al., 2018). The Southern Hemisphere Westerlies winds (SWW) reached their southernmost position from ~6 to 2 ka BP (Fig. 5H) (Voigt et al., 2015) and core SWW intensified from ~5 ka BP (Fig. 5I) (Lamy et al., 2010), comparing well to an increase in $^{10}Be/^{9}Be$ ratios between 4.1 and 3.6 ka BP in L. Maruwan Oike and L. Skallen (Fig. 5A). This suggests variations in the SWW, possibly linked to ENSO variability as previously discussed, could have pushed the Antarctic Coastal Current further south whilst also increasing the penetration of warm waters into the Southern Ocean (Delworth and Zeng, 2008; Voigt et al., 2016). This would have led to warming and increased intrusion of the CDW onto the Antarctic shelf (Crosta et al., 2018) leading to the melting of glaciers along the Soya Coast. This is supported by foraminifera abundance data in marine sediment cores from the eastern part of Lützow-Holm Bay which indicate the incursion of warm, $CaCO_3$-saturated and nutrient-rich CDW waters during the Late Holocene (Igarashi et al., 2001).

The transition from the Middle to Late Holocene at 4.2 ka BP is marked by widespread drought conditions in mid-continent North America, the Mediterranean, the Middle East and parts of Asia and drier climate regimes in Africa and South America often associated with societal upheaval and the collapse of civilisations (Walker et al., 2012). A recent compilation of low-latitude sea-level reconstructions indicate that a 3–4 m of global sea level equivalent ice sheet melting occurred during the Mid Holocene, terminating at around 3 to 4 ka, due to the retreat of the Antarctic and/or Greenland ice sheets (Yokoyama et al., 2019a). This study supports the notion of meltwater contribution to sea-level rise from the EAIS between 4.1 and 3.6 ka BP.

6. Conclusions

The reactive ^{10}Be and ^{9}Be abundance of sediments from L. Maruwan Oike and L. Skallen along the Soya Coast of Lützow-Holm Bay, East Antarctica, were measured to determine the meltwater and weathering response of the Rundvåg and Skallen glaciers to climatic change during the Mid to Late Holocene. When compared with previously analysed elemental abundances, Be isotopes appear to be controlled by freshwater and terrigenous inputs from nearby glaciers with little influence from atmospheric or marine sources. Both lakes record a substantial increase in $^{10}Be/^{9}Be$ ratios between ~4.1 and ~3.6 ka BP reflecting a <730% increase in meltwater flux over this period. This coincides with evidence of glacial discharge to Prydz Bay, offshore Adélie Land, the Ross Sea and the west Antarctic Peninsula indicating glacial melting along the Soya Coast was part of a circum-Antarctic phenomena. Echoing previous studies, we suggest a southward migration and intensification of SWW and deepening of the Circumpolar Trough led to the upwelling and incursion of relatively warm CDW to Lützow-Holm Bay. This may have been compounded by higher subsurface warming under increasing insolation at southern polar latitudes during the Late Holocene.

Finally, despite elucidating the deglacial history along part of the

Soya Coast in this study, L. Maruwan Oike and L. Skallen form a small part of the larger Soya and Shirase drainage basins, and the Rundvåg and Skallen glaciers only represent a fraction of potential meltwater flux to Lützow-Holm Bay. Analysis of Be isotopes in lake sediments from Lake Yumi Ike, Lake O-Ike, Lake Ura Ike, Lake Higashi Ike and/or Lake Nishi Ike on the Ongul Islands and Lake Mago Ike, Lake Kobachi Ike and/or Lake Oyako on the Skarvsnes peninsula (Fig. 1B) would allow the reconstruction of meltwater history further north along the Soya Coast. Moreover, Be isotope analysis of marine sediments from Lützow-Holm Bay, such as those collected during the 22nd and 23rd Japanese Antarctic Research Expeditions (JARE-22, 1980 to 1982; JARE-33, 1991–1993), would help constrain the meltwater history of the Shirase Glacier and the timing and extent of CDW incursion during the Holocene. Together this would provide a better understanding of EAIS response to oceanic forcing and help constrain the potential contribution of Antarctic glacial retreat to global sea-level during the Mid to Late Holocene.

Declaration of competing interest

The authors declare that they have no known competing financial interests or personal relationships that could have appeared to influence the work reported in this paper.

Acknowledgements

We thank M. Fukui (Hokkaido Univ.), T. Sato (Hiroshima Univ.) and S. Imura (Natl. Inst. Polar Res.) for their support of field survey and sampling procedures, T. Sawagaki (Hokkaido Univ.) for the onsite field guide and members of the 47th Japan Antarctica Research Expedition for their logistical assistance. A.D. Sproson and Y. Yokoyama would like to thank the Japan Society for the Promotion of Science (JSPS) for supporting this study through their postdoctoral fellowships (PE17712 and P18791) and Grants-in-Aid (KAKENHI) for Scientific Research (20H00193 and 18F18791). Finally, we would like to thank Prof. Colm O'Cofaigh (Durham University), Dr. Stephen Roberts (British Antarctic Survey) and Dr. van der Bilt (University of Bergen) for their constructive and thoughtful reviews which greatly improved this manuscript.

References

Anderson, J.B., Shipp, S.S., Lowe, A.L., Wellner, J.S., Mosola, A.B., 2002. The antarctic ice sheet during the last glacial Maximum and its subsequent retreat history: a review. Quat. Sci. Rev. 21, 49–70.

Baroni, M., Bard, E., Petit, J.-R., Magand, O., Bourles, D., 2011. Volcanic and solar activity, and atmospheric circulation influences on cosmogenic 10Be fallout at Vostok and Concordia (Antarctica) over the last 60 years. Geochem. Cosmochim. Acta 75, 7132–7145.

Behrens, B., Miyairi, Y., Sproson, A.D., Yamane, M., Yokoyama, Y., 2019. Meltwater discharge during the Holocene from the Wilkes subglacial basin revealed by beryllium isotope analysis of marine sediments. J. Quat. Sci. 34, 603–608.

Bentley, M.J., Ó Cofaigh, C., Anderson, J.B., Conway, H., Davies, B., Graham, A.G.C., Hillenbrand, C.-D., Hodgson, D.A., Jamieson, S.S.R., Larter, R.D., Mackintosh, A., Smith, J.A., Verleyen, E., Ackert, R.P., Bart, P.J., Berg, S., Brunstein, D., Canals, M., Colhoun, E.A., Crosta, X., Dickens, W.A., Domack, E., Dowdeswell, J.A., Dunbar, R., Ehrmann, W., Evans, J., Favier, V., Fink, D., Fogwill, C.J., Glasser, N.F., Gohl, K., Golledge, N.R., Goodwin, I., Gore, D.B., Greenwood, S.L., Hall, B.L., Hall, K., Hedding, D.W., Hein, A.S., Hocking, E.P., Jakobsson, M., Johnson, J.S., Jomelli, V., Jones, R.S., Klages, J.P., Kristoffersen, Y., Kuhn, G., Leventer, A., Licht, K., Lilly, K., Lindow, J., Livingstone, S.J., Massé, G., McGlone, M.S., McKay, R.M., Melles, M., Miura, H., Mulvaney, R., Nel, W., Nitsche, F.O., O'Brien, P.E., Post, A.L., Roberts, S.J., Saunders, K.M., Selkirk, P.M., Simms, A.R., Spiegel, C., Stolldorf, T.D., Sugden, D.E., van der Putten, N., van Ommen, T., Verfaillie, D., Vyverman, W., Wagner, B., White, D.A., Witus, A.E., Zwartz, D., 2014. A community-based geological reconstruction of antarctic ice sheet deglaciation since the last glacial Maximum. Quat. Sci. Rev. 100, 1–9.

Bindschadler, R., Vornberger, P., Fleming, A., Fox, A., Mullins, J., Binnie, D., Paulsen, S.J., Granneman, B., Gorodetzky, D., 2008. The landsat image mosaic of Antarctica. Rem. Sens. Environ. 112, 4214–4226.

Bourles, D., Raisbeck, G.M., Yiou, F., 1989. 10Be and 9Be in marine sediments and their potential for dating. Geochem. Cosmochim. Acta 53, 443–452.

Brown, E.T., Measures, C.I., Edmond, J.M., Bourlès, D.L., Raisbeck, G.M., Yiou, F., 1992. Continental inputs of beryllium to the oceans. Earth Planet Sci. Lett. 114, 101–111.

Brown, G.H., 2002. Glacier meltwater hydrochemistry. Appl. Geochem. 17, 855–883.

Choi, Y., Kim, K.J., Cheong, D., Kim, Y.H., 2014. Paleoclimate signals of lake Hovsgol, Mongolia, over the last 19,000 Years using authigenic beryllium isotopes. Radiocarbon 56, 1139–1150.

Conroy, J.L., Overpeck, J.T., Cole, J.E., Shanahan, T.M., Steinitz-Kannan, M., 2008. Holocene changes in eastern tropical Pacific climate inferred from a Galápagos lake sediment record. Quat. Sci. Rev. 27, 1166–1180.

Crespin, J., Yam, R., Crosta, X., Massé, G., Schmidt, S., Campagne, P., Shemesh, A., 2014. Holocene glacial discharge fluctuations and recent instability in East Antarctica. Earth Planet Sci. Lett. 394, 38–47.

Crosta, X., Crespin, J., Swingedouw, D., Marti, O., Masson-Delmotte, V., Etourneau, J., Goosse, H., Braconnot, P., Yam, R., Brailovski, I., Shemesh, A., 2018. Ocean as the main driver of Antarctic ice sheet retreat during the Holocene. Global Planet. Change 166, 62–74.

DeConto, R.M., Pollard, D., 2016. Contribution of Antarctica to past and future sea-level rise. Nature 531, 591–597.

Delworth, T.L., Zeng, F., 2008. Simulated impact of altered Southern Hemisphere winds on the Atlantic meridional overturning circulation. Geophys. Res. Lett. 35.

Flower, B.P., Kennett, J.P., 1994. The middle Miocene climatic transition: east Antarctic ice sheet development, deep ocean circulation and global carbon cycling. Palaeogeogr. Palaeoclimatol. Palaeoecol. 108, 537–555.

Frank, M., Porcelli, D., Andersson, P., Baskaran, M., Björk, G., Kubik, P.W., Hattendorf, B., Guenther, D., 2009. The dissolved Beryllium isotope composition of the Arctic Ocean. Geochem. Cosmochim. Acta 73, 6114–6133.

Fretwell, P., Pritchard, H.D., Vaughan, D.G., Bamber, J.L., Barrand, N.E., Bell, R., Bianchi, C., Bingham, R.G., Blankenship, D.D., Casassa, G., Catania, G., Callens, D., Conway, H., Cook, A.J., Corr, H.F.J., Damaske, D., Damm, V., Ferraccioli, F., Forsberg, R., Fujita, S., Gim, Y., Gogineni, P., Griggs, J.A., Hindmarsh, R.C.A., Holmlund, P., Holt, J.W., Jacobel, R.W., Jenkins, A., Jokat, W., Jordan, T., King, E.C., Kohler, J., Krabill, W., Riger-Kusk, M., Langley, K.A., Leitchenkov, G., Leuschen, C., Luyendyk, B.P., Matsuoka, K., Mouginot, J., Nitsche, F.O., Nogi, Y., Nost, O.A., Popov, S.V., Rignot, E., Rippin, D.M., Rivera, A., Roberts, J., Ross, N., Siegert, M.J., Smith, A.M., Steinhage, D., Studinger, M., Sun, B., Tinto, B.K., Welch, B.C., Wilson, D., Young, D.A., Xiangbin, C., Zirizzotti, A., 2013. Bedmap2: improved ice bed, surface and thickness datasets for Antarctica. Cryosphere 7, 375–393.

Gehrels, R., 2010. sea-level changes since the last glacial Maximum: an appraisal of the IPCC fourth assessment report. J. Quat. Sci. 25, 26–38.

Hayashi, M., Yoshida, Y., 1994. Holocene raised beaches in the Lützow-Holm Bay region, East Antarctica. Mem. Natl. Inst. Polar Res. - Special Issue 50, 49–84.

Hogg, A.G., Hua, Q., Blackwell, P.G., Niu, M., Buck, C.E., Guilderson, T.P., Heaton, T.J., Palmer, J.G., Reimer, P.J., Reimer, R.W., 2013. SHCal13 Southern Hemisphere calibration, 0–50,000 years cal BP. Radiocarbon 55, 1889–1903.

Hughen, K.A., Baillie, M.G.L., Bard, E., Warren Beck, J., Bertrand, C.J.H., Blackwell, P.G., Buck, C.E., Burr, G.S., Cutler, K.B., Damon, P.E., Edwards, R.L., Fairbanks, R.G., Friedrich, M., Guilderson, T.P., Kromer, B., McCormac, G., Manning, S., Bronk Ramsey, C., Reimer, P.J., Reimer, R.W., Remmele, S., Southon, J.R., Stuiver, M., Talamo, S., Taylor, F.W., Van der Plicht, J., Weyhenmeyer, C.E., 2004. Marine04 marine radiocarbon age calibration, 0–26 cal kyr bp. Radiocarbon 46, 1059–1086.

Igarashi, A., Numanami, H., Tsuchiya, Y., Fukuchi, M., 2001. Bathymetric distribution of fossil foraminifera within marine sediment cores from the eastern part of Lützow-Holm Bay, East Antarctica, and its paleoceanographic implications. Mar. Micropaleontol. 42, 125–162.

Imura, S., Bando, T., Seto, K., Ohtani, S., Kudoh, S., Kanda, H., 2003. Distribution of Aquatic Mosses in the Soya Coast Region, East Antarctica.

Ingólfsson, Ó., Hjort, C., Berkman, P.A., Björck, S., Colhoun, E., Goodwin, I.D., Hall, B., Hirakawa, K., Melles, M., Möller, P., 1998. Antarctic Glacial History since the Last Glacial Maximum: an Overview of the Record on Land.

Institute, G.S., 1984. Rundvågshetta: the Principal Part. Map Compilation from Air Photography, Controlled by Triangulation Points Established by JARE, 1971 and 1974.

Johnson, J.S., Bentley, M.J., Smith, J.A., Finkel, R.C., Rood, D.H., Gohl, K., Balco, G., Larter, R.D., Schaefer, J.M., 2014. Rapid thinning of pine island glacier in the early Holocene. Science 343, 999.

Jones, R.S., Norton, K.P., Mackintosh, A.N., Anderson, J.T.H., Kubik, P., Vockenhuber, C., Wittmann, H., Fink, D., Wilson, G.S., Golledge, N.R., McKay, R., 2017. Cosmogenic nuclides constrain surface fluctuations of an East Antarctic outlet glacier since the Pliocene. Earth Planet Sci. Lett. 480, 75–86.

Kawamata, M., Suganuma, Y., Doi, K., Misawa, K., Hirabayashi, M., Hattori, A., Sawagaki, T., 2020. Abrupt Holocene ice-sheet thinning along the southern Soya Coast, Lützow-Holm Bay, East Antarctica, revealed by glacial geomorphology and surface exposure dating. Quat. Sci. Rev. 247, 106540.

Kim, K.J., Zolitschka, B., Jull, A.J.T., Ohlendorf, C., Haberzettl, T., Matsuzaki, H., 2012. Tracing environmental change in southern Patagonia using beryllium isotopes, Laguna Potrok Aike, Argentina. Quat. Geochronol. 9, 27–33.

Knudsen, M.F., Henderson, G.M., Frank, M., Mac Niocaill, C., Kubik, P.W., 2008. In-phase anomalies in Beryllium-10 production and palaeomagnetic field behaviour during the Iceland Basin geomagnetic excursion. Earth Planet Sci. Lett. 265, 588–599.

Kohl, C., Nishiizumi, K., 1992. Chemical isolation of quartz for measurement of in-

situ-produced cosmogenic nuclides. Geochem. Cosmochim. Acta 56, 3583–3587.
Ku, T., Kusakabe, M., Measures, C., Southon, J., Cusimano, G., Vogel, J., Nelson, D., Nakaya, S., 1990. Beryllium isotope distribution in the western north atlantic: a comparison to the pacific. Deep sea Research Part A. Oceanogr. Res. Pap. 37, 795–808.
Kudoh, S., Tanabe, Y., 2014. Limnology and ecology of lakes along the sôya coast, east Antarctica. 极地研究 25, 75–91.
Kusakabe, M., Ku, T., Southon, J., Vogel, J., Nelson, D., Measures, C., Nozaki, Y., 1987. Distribution of10Be and9Be in the pacific ocean. Earth Planet Sci. Lett. 82, 231–240.
Lal, D., 1991. Cosmic ray labeling of erosion surfaces: in situ nuclide production rates and erosion models. Earth Planet Sci. Lett. 104, 424–439.
Lamy, F., Kilian, R., Arz, H.W., Francois, J.-P., Kaiser, J., Prange, M., Steinke, T., 2010. Holocene changes in the position and intensity of the southern westerly wind belt. Nat. Geosci. 3, 695–699.
Lilly, K., Fink, D., Fabel, D., Lambeck, K., 2010. Pleistocene dynamics of the interior East Antarctic ice sheet. Geology 38, 703–706.
Lougheed, B.C., Obrochta, S.P., 2019. A rapid, deterministic age-depth modeling routine for geological sequences with inherent depth uncertainty. Paleoceanogr. Paleoclimatol. 34, 122–133.
Lythe, M.B., Vaughan, D.G., 2001. BEDMAP: a new ice thickness and subglacial topographic model of Antarctica. J. Geophys. Res.: Solid Earth 106, 11335–11351.
Mackintosh, A.N., Verleyen, E., O'Brien, P.E., White, D.A., Jones, R.S., McKay, R., Dunbar, R., Gore, D.B., Fink, D., Post, A.L., Miura, H., Leventer, A., Goodwin, I., Hodgson, D.A., Lilly, K., Crosta, X., Golledge, N.R., Wagner, B., Berg, S., van Ommen, T., Zwartz, D., Roberts, S.J., Vyverman, W., Masse, G., 2014. Retreat history of the east antarctic ice sheet since the last glacial Maximum. Quat. Sci. Rev. 100, 10–30.
Masson, V., Vimeux, F., Jouzel, J., Morgan, V., Delmotte, M., Ciais, P., Hammer, C., Johnsen, S., Lipenkov, V.Y., Mosley-Thompson, E., 2000. Holocene climate variability in Antarctica based on 11 ice-core isotopic records. Quat. Res. 54, 348–358.
Masson-Delmotte, V., Buiron, D., Ekaykin, A., Frezzotti, M., Gallée, H., Jouzel, J., Krinner, G., Landais, A., Motoyama, H., Oerter, H., Pol, K., Pollard, D., Ritz, C., Schlosser, E., Sime, L.C., Sodemann, H., Stenni, B., Uemura, R., Vimeux, F., 2011. A comparison of the present and last interglacial periods in six Antarctic ice cores. Clim. Past 7, 397–423.
Matsuoka, K., Skoglund, A., Roth, G., Tronstad, S., Melvær, Y., 2018. Quantarctica. Norwegian Polar Institute, vol. 10.
Matsuzaki, H., Nakano, C., Tsuchiya, Y., Kato, K., Maejima, Y., Miyairi, Y., Wakasa, S., Aze, T., 2007. Multi-nuclide AMS performances at MALT. Nucl. Instrum. Methods Phys. Res. Sect. B Beam Interact. Mater. Atoms 259, 36–40.
Measures, C., Ku, T., Luo, S., Southon, J., Xu, X., Kusakabe, M., 1996. The distribution of 10Be and 9Be in the south atlantic. Deep Sea Res. Oceanogr. Res. Pap. 43, 987–1009.
Melles, M., Brigham-Grette, J., Minyuk, P.S., Nowaczyk, N.R., Wennrich, V., DeConto, R.M., Anderson, P.M., Andreev, A.A., Coletti, A., Cook, T.L., 2012. 2.8 million years of Arctic climate change from Lake El'gygytgyn, NE Russia. Science 337, 315–320.
Minyuk, P., Borkhodoev, V., Wennrich, V., 2014. Inorganic geochemistry data from Lake El'gygytgyn sediments: marine isotope stages 6-11. Clim. Past 10, 467.
Miura, H., Maemoku, H., Igarashi, A., Moriwaki, K., 1998. Late Quaternary Raised Beach Deposits and Radiocarbon Dates of Marine Fossils Around Lützow-Holm Bay. Special map series of National Institute of Polar Research.
Miura, H., Maemoku, H., Moriwaki, K., 2002. Holocene raised beach stratigraphy and sea-level history of kizahasi beach, Skarvsnes, luetzow-holm bay. In: Antarctica, Antarctica at the Close of a Millennium: Proceedings of the 8th International Symposium on Antarctic Earth Sciences, Wellington 1999.
Mouginot, J., Scheuchl, B., Rignot, E., 2012. Mapping of ice motion in Antarctica using synthetic-aperture radar data. Rem. Sens. 4, 2753–2767.
Moy, C.M., Seltzer, G.O., Rodbell, D.T., Anderson, D.M., 2002. Variability of El niño/southern oscillation activity at millennial timescales during the Holocene epoch. Nature 420, 162–165.
Nakamura, K., Yamanokuchi, T., Doi, K., Shibuya, K., 2016. Net mass balance calculations for the Shirase Drainage Basin, east Antarctica, using the mass budget method. Polar Sci. 10, 111–122.
Nishiizumi, K., Imamura, M., Caffee, M.W., Southon, J.R., Finkel, R.C., McAninch, J., 2007. Absolute calibration of 10Be AMS standards. Nucl. Instrum. Methods Phys. Res. Sect. B Beam Interact. Mater. Atoms 258, 403–413.
Nishiizumi, K., Kohl, C.P., Arnold, J.R., Klein, J., Fink, D., Middleton, R., 1991. Cosmic ray produced 10Be and 26Al in Antarctic rocks: exposure and erosion history. Earth Planet Sci. Lett. 104, 440–454.
Pike, J., Swann, G.E.A., Leng, M.J., Snelling, A.M., 2013. Glacial discharge along the West antarctic peninsula during the Holocene. Nat. Geosci. 6, 199–202.
Pollard, D., DeConto, R.M., 2009. Modelling West Antarctic ice sheet growth and collapse through the past five million years. Nature 458, 329–332.
Rahaman, W., Wittmann, H., von Blanckenburg, F., 2017. Denudation rates and the degree of chemical weathering in the Ganga River basin from ratios of meteoric cosmogenic 10Be to stable 9Be. Earth Planet Sci. Lett. 469, 156–169.
Raisbeck, G., Yiou, F., Jouzel, J., Stocker, T., 2007. Direct north-south synchronization of abrupt climate change record in ice cores using Beryllium 10. Clim. Past 3, 541–547.
Raisbeck, G.M., Yiou, F., 1985. 10Be in polar ice and atmospheres. Ann. Glaciol. 7, 138–140.
Reimer, P.J., Baillie, M.G., Bard, E., Bayliss, A., Beck, J.W., Blackwell, P.G., Ramsey, C.B., Buck, C.E., Burr, G.S., Edwards, R.L., 2009. IntCal09 and Marine09 radiocarbon age calibration curves, 0–50,000 years cal BP. Radiocarbon 51, 1111–1150.
Reimer, P.J., Bard, E., Bayliss, A., Beck, J.W., Blackwell, P.G., Ramsey, C.B., Buck, C.E., Cheng, H., Edwards, R.L., Friedrich, M., 2013. IntCal13 and Marine13 radiocarbon age calibration curves 0–50,000 years cal BP. Radiocarbon 55, 1869–1887.
Rignot, E., Jacobs, S., Mouginot, J., Scheuchl, B., 2013. Ice-shelf melting around Antarctica. Science 341, 266.
Rignot, E., Mouginot, J., Scheuchl, B., 2011. Ice flow of the antarctic ice sheet. Science 333, 1427.
Rudd, R.C., 2019. Lake Sediment Archives of Late Holocene Climate Variability in Lutzow-Holm Bay, East Antarctica.
Rudd, R.C., Tyler, J.J., Tibby, J., Yokoyama, Y., Tavernier, I., Verleyen, E., Fukui, M., Takano, Y., 2016. A diatom-inferred record of lake variability during the last 900 years in Lützow–Holm Bay, East Antarctica. J. Quat. Sci. 31, 114–125.
Sapota, T., Aldahan, A., Al-Aasm, I.S., 2006. Sedimentary facies and climate control on formation of vivianite and siderite microconcretions in sediments of Lake Baikal, Siberia. J. Paleolimnol. 36, 245–257.
Sawagaki, T., Hirakawa, K., 1997. Erosion of bedrock by subglacial meltwater, Soya coast, east Antarctica. Geogr. Ann. Phys. Geogr. 79, 223–238.
Scherer, R.P., Aldahan, A., Tulaczyk, S., Possnert, G., Engelhardt, H., Kamb, B., 1998. Pleistocene collapse of the west antarctic ice sheet. Science 281, 82.
Shiraishi, K., 2007. Activities of the Summer Season of the 47th Japanese Antarctic Research Expedition, 2005-2006 (In Japanese). ANTARCTIC RECORD-TOKYO-, pp. 51–95.
Simon, Q., Thouveny, N., Bourlès, D.L., Nuttin, L., Hillaire-Marcel, C., St-Onge, G., 2016. Authigenic 10Be/9Be ratios and 10Be-fluxes (230Thxs-normalized) in central Baffin Bay sediments during the last glacial cycle: paleoenvironmental implications. Quat. Sci. Rev. 140, 142–162.
Sjunneskog, C., Scherer, R., Aldahan, A., Possnert, G., 2007. 10Be in glacial marine sediment of the Ross Sea, Antarctica, a potential tracer of depositional environment and sediment chronology. Nucl. Instrum. Methods Phys. Res. Sect. B Beam Interact. Mater. Atoms 259, 576–583.
Small, D., Bentley, M.J., Jones, R.S., Pittard, M.L., Whitehouse, P.L., 2019. Antarctic ice sheet palaeo-thinning rates from vertical transects of cosmogenic exposure ages. Quat. Sci. Rev. 206, 65–80.
Spector, P., Stone, J., Cowdery, S.G., Hall, B., Conway, H., Bromley, G., 2017. Rapid early-holocene deglaciation in the Ross Sea, Antarctica. Geophys. Res. Lett. 44, 7817–7825.
Sproson, A.D., Aze, T., Behrens, B., Yokoyama, Y., 2021. Initial measurement of beryllium-9 using high-resolution inductively coupled plasma mass spectrometry allows for more precise applications of the beryllium isotope system within the Earth Sciences. Rapid Commun. Mass Spectrom. 35, e9059. https://doi.org/10.1002/rcm.9059.
Stuiver, M., Reimer, P.J., Braziunas, T.F., 1998. High-precision radiocarbon age calibration for terrestrial and marine samples. Radiocarbon 40, 1127–1151.
Takada, M., Tani, A., Miura, H., Moriwaki, K., Nagatomo, T., 2003. ESR dating of fossil shells in the Lützow-Holm Bay region, East Antarctica. Quat. Sci. Rev. 22, 1323–1328.
Takano, Y., Kojima, H., Takeda, E., Yokoyama, Y., Fukui, M., 2015. Biogeochemistry and limnology in Antarctic subglacial weathering: molecular evidence of the linkage between subglacial silica input and primary producers in a perennially ice-covered lake. Progress Earth Planet. Sci. 2–8.
Takano, Y., Tyler, J.J., Kojima, H., Yokoyama, Y., Tanabe, Y., Sato, T., Ogawa, N.O., Ohkouchi, N., Fukui, M., 2012. Holocene lake development and glacial-isostatic uplift at Lake Skallen and Lake Oyako, Lützow-Holm Bay, East Antarctica: based on biogeochemical facies and molecular signatures. Appl. Geochem. 27, 2546–2559.
Takano, Y., Yokoyama, Y., Tyler, J.J., Kojima, H., Fukui, M., Sato, T., Ogawa, N., Suzuki, N., Kitazato, H., Ohkouchi, N., 2010. Crustal uplifting rate associated with late-Holocene glacial-isostatic rebound at Skallen and Skarvsnes, Lützow-Holm Bay, East Antarctica: evidence of a synchrony in sedimentary and biological facies on geological setting. Biogeosci. Discuss. 7.
Tatsumi, T., Kizaki, K., 1969. Geology of the Lützow-Holm Bay Region and the "Yamato Mountains"(Queen Fabiola Mountains). Geog. Soc. Antarctic Map Folio Series, Folio.
Valletta, R.D., Willenbring, J.K., Lewis, A.R., Ashworth, A.C., Caffee, M., 2015. Extreme decay of meteoric beryllium-10 as a proxy for persistent aridity. Sci. Rep. 5, 17813.
Valletta, R.D., Willenbring, J.K., Passchier, S., Elmi, C., 2018. 10Be/9Be ratios reflect Antarctic Ice Sheet freshwater discharge during Pliocene warming. Paleoceanogr. Paleoclimatol. 33, 934–944.
Verleyen, E., Tavernier, I., Hodgson, D.A., Whitehouse, P.L., Kudoh, S., Imura, S., Heirman, K., Bentley, M.J., Roberts, S.J., De Batist, M., Sabbe, K., Vyverman, W., 2017. Ice sheet retreat and glacio-isostatic adjustment in Lützow-Holm Bay, East Antarctica. Quat. Sci. Rev. 169, 85–98.
Voigt, I., Chiessi, C.M., Piola, A.R., Henrich, R., 2016. Holocene changes in antarctic intermediate water flow strength in the southwest atlantic. Palaeogeogr. Palaeoclimatol. Palaeoecol. 463, 60–67.
Voigt, I., Chiessi, C.M., Prange, M., Mulitza, S., Groeneveld, J., Varma, V., Henrich, R., 2015. Holocene shifts of the southern westerlies across the South Atlantic. Paleoceanography 30, 39–51.
von Blanckenburg, F., Bouchez, J., 2014. River fluxes to the sea from the ocean's 10Be/9Be ratio. Earth Planet Sci. Lett. 387, 34–43.
Von Blanckenburg, F., Bouchez, J., Ibarra, D.E., Maher, K., 2015. Stable runoff and

weathering fluxes into the oceans over Quaternary climate cycles. Nat. Geosci. 8, 538–542.
von Blanckenburg, F., Bouchez, J., Wittmann, H., 2012. Earth surface erosion and weathering from the 10Be (meteoric)/9Be ratio. Earth Planet Sci. Lett. 351, 295–305.
Walker, M.J., Berkelhammer, M., Björck, S., Cwynar, L.C., Fisher, D.A., Long, A.J., Lowe, J.J., Newnham, R.M., Rasmussen, S.O., Weiss, H., 2012. Formal subdivision of the Holocene series/epoch: a discussion paper by a working group of INTIMATE (integration of ice-core, marine and terrestrial records) and the subcommission on quaternary stratigraphy (international commission on stratigraphy). J. Quat. Sci. 27, 649–659.
Watanabe, T., Kojima, H., Takano, Y., Fukui, M., 2013. Diversity of sulfur-cycle prokaryotes in freshwater lake sediments investigated using aprA as the functional marker gene. Syst. Appl. Microbiol. 36, 436–443.
White, D.A., Fink, D., Post, A.L., Simon, K., Galton-Fenzi, B., Foster, S., Fujioka, T., Jeromson, M.R., Blaxell, M., Yokoyama, Y., 2019. Beryllium isotope signatures of ice shelves and sub-ice shelf circulation. Earth Planet Sci. Lett. 505, 86–95.
Whitlock, C., Dean, W., Rosenbaum, J., Stevens, L., Fritz, S., Bracht, B., Power, M., 2008. A 2650-year-long record of environmental change from northern Yellowstone National Park based on a comparison of multiple proxy data. Quat. Int. 188, 126–138.
Willenbring, J.K., von Blanckenburg, F., 2010. Meteoric cosmogenic Beryllium-10 adsorbed to river sediment and soil: applications for Earth-surface dynamics. Earth Sci. Rev. 98, 105–122.
Wittmann, H., von Blanckenburg, F., Bouchez, J., Dannhaus, N., Naumann, R., Christl, M., Gaillardet, J., 2012. The dependence of meteoric 10Be concentrations on particle size in Amazon River bed sediment and the extraction of reactive 10Be/9Be ratios. Chem. Geol. 318, 126–138.
Yamane, M., Yokoyama, Y., Abe-Ouchi, A., Obrochta, S., Saito, F., Moriwaki, K., Matsuzaki, H., 2015. Exposure age and ice-sheet model constraints on Pliocene East Antarctic ice sheet dynamics. Nat. Commun. 6, 7016.
Yamane, M., Yokoyama, Y., Miura, H., Maemoku, H., Iwasaki, S., Matsuzaki, H., 2011. The last deglacial history of Lützow-Holm Bay, East Antarctica. J. Quat. Sci. 26, 3–6.
Yokoyama, Y., Anderson, J.B., Yamane, M., Simkins, L.M., Miyairi, Y., Yamazaki, T., Koizumi, M., Suga, H., Kusahara, K., Prothro, L., Hasumi, H., Southon, J.R., Ohkouchi, N., 2016. Widespread collapse of the Ross ice shelf during the late Holocene. Proc. Natl. Acad. Sci. Unit. States Am. 113, 2354.
Yokoyama, Y., Hirabayashi, S., Goto, K., Okuno, J.i., Sproson, A.D., Haraguchi, T., Ratnayake, N., Miyairi, Y., 2019a. Holocene Indian Ocean sea level, Antarctic melting history and past Tsunami deposits inferred using sea level reconstructions from the Sri Lankan, Southeastern Indian and Maldivian coasts. Quat. Sci. Rev. 206, 150–161.
Yokoyama, Y., Miyairi, Y., Aze, T., Yamane, M., Sawada, C., Ando, Y., de Natris, M., Hirabayashi, S., Ishiwa, T., Sato, N., Fukuyo, N., 2019b. A single stage accelerator mass Spectrometry at the atmosphere and Ocean Research Institute, the university of Tokyo. Nucl. Instrum. Methods Phys. Res. Sect. B Beam Interact. Mater. Atoms 455, 311–316.
Yokoyama, Y., Miyairi, Y., Matsuzaki, H., Tsunomori, F., 2007. Relation between acid dissolution time in the vacuum test tube and time required for graphitization for AMS target preparation. Nucl. Instrum. Methods Phys. Res. Sect. B Beam Interact. Mater. Atoms 259, 330–334.
Yokoyama, Y., Yamane, M., Nakamura, A., Miyairi, Y., Horiuchi, K., Aze, T., Matsuzaki, H., Shirahama, Y., Ando, Y., 2019c. In-situ and meteoric 10Be and 26Al measurements: improved preparation and application at the University of Tokyo. Nucl. Instrum. Methods Phys. Res. Sect. B Beam Interact. Mater. Atoms 455, 260–264.
Young, G.M., Nesbitt, H.W., 1998. Processes controlling the distribution of Ti and Al in weathering profiles, siliciclastic sediments and sedimentary rocks. J. Sediment. Res. 68, 448–455.